Effect of an internal rotating current on low-frequency inductively coupled plasmas

E. L. Tsakadze,[1] K. N. Ostrikov,[1–4,*] S. Xu,[1,†] I. R. Jones,[2] R. Storer,[2] M. Y. Yu,[3] and S. Lee[1]
[1]*Plasma Processing Laboratory, NIE, Nanyang Technological University, 1 Nanyang Walk, 637616 Singapore*
[2]*Department of Physics, Flinders University of South Australia, GPO Box 2100, Adelaide SA 5001, Australia*
[3]*Institute for Theoretical Physics I, Ruhr University, D-44780 Bochum, Germany*
[4]*Department of Electrical Engineering, Nagoya University, Nagoya 464-8603, Japan*
(Received 11 September 2000; published 22 March 2001)

The effect of an internal low-frequency rotating current on inductively coupled plasmas in cylindrical chambers is studied. The electromagnetic field structure, power density distribution, the plasma density, and the operating regimes of the discharge are investigated using electrodynamic, power, and particle balance equations. It is shown that the rotating current sheet can dramatically improve the uniformity of the electromagnetic fields and the power transferred to the plasma electrons from that of conventional low-frequency inductively coupled plasma sources with external flat spiral inductive coils.

DOI: 10.1103/PhysRevE.63.046402 PACS number(s): 52.80.−s

I. INTRODUCTION

In recent years, radio frequency (RF) plasmas have become increasingly attractive as efficient sources of low-temperature plasmas for industrial applications and laboratory experiments. In particular, the RF glow discharges have been proven to be superior in producing large-area large-volume plasmas for semiconductor manufacturing, as well as material processing and syntheses. Furthermore, high plasma density and uniformity over large areas and volumes are crucial for improving the efficiency of plasma processing [1,2] and RF current drive [3]. Typically, plasma densities of 10^{10}–$10^{12}\,\mathrm{cm}^{-3}$ with RF powers ~ 1–2 kW have been achieved in several types of RF plasma devices including inductively coupled [4] and helicon-wave driven [5] plasma sources, as well as compact spherical tori [6].

How the plasma is generated in various RF devices can be quite different and is mainly determined by the corresponding dominant power transfer mechanism. For instance, inductively coupled plasmas (ICPs) are usually produced by external or internal currents driven by coils of various configurations. In compact toroidal devices RF currents are often excited by a combination of external inductive coils. Depending on the coil configuration and the operating regime, the currents excited can be of either constant or spatially varying phases. In particular, in a compact spherical plasma device, the constant phase case has been referred as oscillating-magnetic field current drive [7], and the spatially varying case as rotating-magnetic field current drive [3,8]. The merit of this scheme is the excitation of steady toroidal plasma currents and high-density uniform plasmas in large volumes [3].

Here, we propose the possibility of efficient high-density uniform plasma generation by an internal rotating RF current in a cylindrical metal vessel. From the basic conservation laws, the spatially averaged plasma densities as functions of the input power and approximate plasma density profiles are computed. Our results show that the uniformity of the electromagnetic fields and power density, a troublesome problem in ICP sources [9], can be improved noticeably by introducing the low-frequency internal rotating current (IRC). The field distribution, the efficiency of power deposition, and the plasma properties are also compared with that of conventional external flat spiral coil ICP sources having the same geometrical size.

The paper is organized as follows. In Sec. II, we study the spatial distribution of electromagnetic fields in a cylindrical metallic chamber filled with rarefied or dense plasma. In Sec. III, the power transferred to the plasma electrons for the IRC configuration is calculated. In Sec. IV, we investigate the particle and power balance, and compute the operating points of the discharge. The results and the effect of the IRC on low-frequency ICPs are discussed in Sec. V. A summary of this work and outlook for future research are given in Sec. VI.

II. ELECTROMAGNETIC FIELDS

In this section, we investigate the distribution of electromagnetic fields in a plasma-filled cylindrical metallic chamber with internal radius R and length $L+\mathcal{L}$. The chamber top is at $z=-\mathcal{L}$, and the chamber bottom is at $z=L$. The plasma is generated by a uniformly distributed RF current sheet which rotates in the azimuthal direction over the circular cross section at $z=0$. The rotating current is given by

$$I_{\mathrm{RF}}=I_0\exp[-i(\omega t-\phi)](\hat{r}+i\hat{\phi}), \tag{1}$$

where $\hat{r}$ and $\hat{\phi}$ are the unit vectors in the radial and azimuthal directions, I_0 and ω are the amplitude and frequency of the RF current, respectively. For calculating the electromagnetic field topography we assume that the plasma is spa-

*Also at the School of Electrical and Electronic Engineering, Nanyang Technological University, Nanyang Avenue, 639798 Singapore. Electronic address: ekostrikov@ntu.edu.sg and ostrikov@tp1.ruhr-uni-bochum.de
†Author to whom correspondence should be addressed. Electronic address: syxu@nie.edu.sg

tially uniform, with densities n_1 and n_2 in the volumes above $(-\mathcal{L}<z<0)$, and below $(0<z<L)$ the current plane, respectively.

We start from the Maxwell equations for the electromagnetic fields in the chamber [10]

$$\nabla\times\mathbf{E}_j=-(1/c)\partial_t\mathbf{H}_j, \tag{2}$$

$$\nabla\times\mathbf{H}_j=(1/c)\partial_t\mathbf{D}_j, \tag{3}$$

where $\mathbf{E}_j$ and $\mathbf{H}_j$ are the electric and magnetic fields in the two different plasma volumes $(j=1,2)$, respectively. Here, $\mathbf{D}_j=\varepsilon_j\mathbf{E}_j$, and $\varepsilon_j=1-\omega_{pj}^2/[\omega(\omega+i\nu_{ej})]$ is the permittivity of the cold plasma, ω_{pj} is the electron plasma frequency, and ν_{ej} is the effective rate of electron collisions.

From the symmetry it is obvious that the TE solutions of (2) and (3) possess E_r and E_ϕ components of the electric field and H_r, H_ϕ, and H_z components of the magnetic field. We impose here the standard boundary conditions of the vanishing of tangential components of electric field and normal components of magnetic field at the side-walls, top, and bottom of the vessel [10]. At the plane $z=0$ there is a jump of the tangential magnetic field proportional to the amplitude of the surface current (1), and the tangential electric field is continuous [10].

From practical considerations, we focus our attention on the field and plasma parameters in $0<z<L$. Assuming that the phase varies as $\sim\exp[-i(\omega t-\phi)]$, for the TE electromagnetic fields in the chamber we obtain

$$H_r^{(2)}=i\sum_{n=1}^{\infty}\frac{\gamma_n^{(2)}\alpha_n}{D_n(TE)}\xi_1^{(2)}(z)\frac{\partial}{\partial r}J_1\left(\frac{\rho'_{1n}r}{R}\right), \tag{4}$$

$$H_\phi^{(2)}=-\frac{1}{r}\sum_{n=1}^{\infty}\frac{\gamma_n^{(2)}\alpha_n}{D_n(TE)}\xi_1^{(2)}(z)J_1\left(\frac{\rho'_{1n}r}{R}\right), \tag{5}$$

$$H_z^{(2)}=-i\sum_{n=1}^{\infty}\frac{\alpha_n}{D_n(TE)}\left(\frac{\rho'_{1n}}{R}\right)^2\xi_2^{(2)}(z)J_1\left(\frac{\rho'_{1n}r}{R}\right), \tag{6}$$

$$E_r^{(2)}=\frac{i\omega}{cr}\sum_{n=1}^{\infty}\frac{\alpha_n}{D_n(TE)}\xi_2^{(2)}(z)J_1\left(\frac{\rho'_{1n}r}{R}\right), \tag{7}$$

$$E_\phi^{(2)}=-\frac{\omega}{c}\sum_{n=1}^{\infty}\frac{\alpha_n}{D_n(TE)}\xi_2^{(2)}(z)\frac{\partial}{\partial r}J_1\left(\frac{\rho'_{1n}r}{R}\right), \tag{8}$$

where

$$\xi_1^{(2)}(z)=\cosh[\gamma_n^{(2)}(L-z)]/\sinh(\gamma_n^{(2)}L),$$

$$\xi_2^{(2)}(z)=\sinh[\gamma_n^{(2)}(L-z)]/\sinh(\gamma_n^{(2)}L),$$

$$\alpha_n=\int_0^R rJ_1\left(\frac{\rho'_{1n}r}{R}\right)f(r)dr/\int_0^R rJ_1^2\left(\frac{\rho'_{1n}r}{R}\right)dr,$$

$$D_n(TE)=\gamma_n^{(1)}\coth(\gamma_n^{(1)}\mathcal{L})+\gamma_n^{(2)}\coth(\gamma_n^{(2)}L),$$

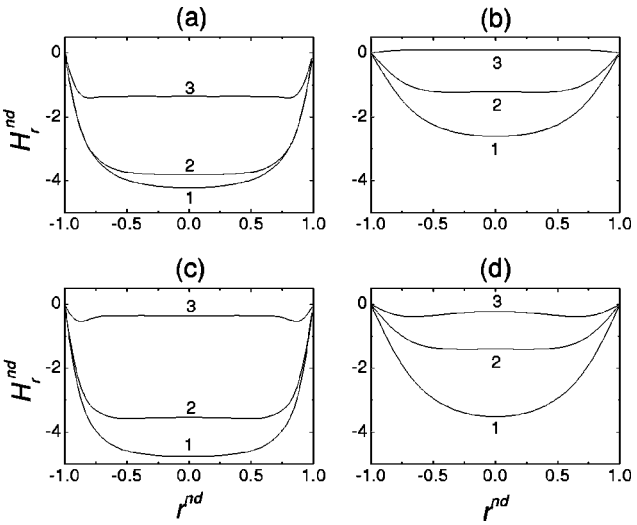

FIG. 1. Nondimensional radial component of magnetic field $H_r^{nd}=\mathrm{Re}(H_r)c/\mathcal{J}$ *versus* dimensionless radial distance $r^{nd}=r/R$ for $\nu_{e2}/\omega=30.0$, $\nu_{e2}/\nu_{e1}=2.0$, $\omega_{p2}/\omega_{p1}=1.5$, and $\mathcal{L}/L=0.25$. Diagrams (a)–(d) correspond to the following azimuthal angles ϕ and dimensionless axial distance $z^{nd}=z/L$: (a) 45°, 0.1; (b) 45°, 0.3; (c) 90°, 0.1, and (d) 90°, 0.3, respectively. Curves 1–3 have been plotted for $n_{e2}=4\times10^{11}\,\mathrm{cm}^{-3}$ (1), $10^{12}\,\mathrm{cm}^{-3}$ (2), and $8\times10^{12}\,\mathrm{cm}^{-3}$ (3), respectively.

$\gamma_n^{(1,2)}=[(\rho'_{1n}/R)^2-(\omega/c)^2\varepsilon_{(1,2)}]^{1/2}$ is the inverse field penetration length, $\partial J_1(\rho'_{1n})/\partial r=0$, $f(r)=(4\pi/c)\mathcal{J}r$, and $\mathcal{J}=I_0/2R$ is a surface current per unit diameter length. Here, the superscripts 1 and 2 correspond to $-\mathcal{L}<z<0$ and $0<z<L$, respectively.

Figs. 1–3 depict the radial profiles of H_r, H_z, and E_ϕ components of the electromagnetic field in the chamber for different plasma densities, axial positions, and azimuthal angles at $t=0$.

The plasma parameters have been taken close to that of the low-frequency (~500 kHz) ICP source [11,12]. It is evident that the electromagnetic field moves towards the plane

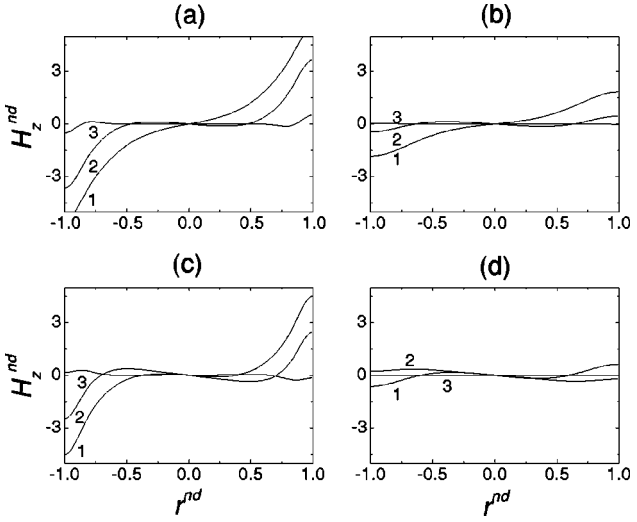

FIG. 2. Same as in Fig. 1, for dimensionless axial magnetic field component $H_z^{nd}=\mathrm{Re}(H_z)c/\mathcal{J}$.

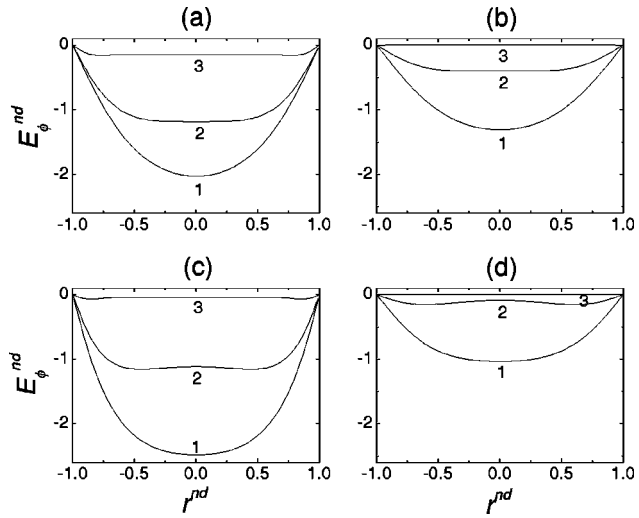

FIG. 3. Same as in Fig. 1, for dimensionless azimuthal electric field component $E_\phi^{nd} = -[\mathrm{Re}(E_\phi)c/\mathcal{J}]\times 10^3$, with $\phi = 90°$ [(a) and (b)], and $\phi = 135°$ [(c) and (d)], respectively.

$z = 0$ as the plasma density increases. This is ubiquitous for many RF plasmas and is attributed to the ''skin effect'' [1], which is collision-dominated in our case since $\nu_{ej}/\omega \gg 1$ [11,12]. One can also see that the H_r and E_ϕ field components vanish at the chamber sidewalls because of the boundary conditions. Furthermore, the radial uniformity of E_ϕ, H_r, and H_z fields in the IRC plasma is better than that in the low-frequency ICP source with similar control parameters [11,12].

The axial profiles of dimensionless azimuthal magnetic and radial electric fields are shown in Fig. 4. The field amplitudes decrease with *z*, and typically vanish at the bottom of the chamber. From Fig. 4 one can estimate the *e*-fold field decay length, which turns out to be ~ 8.86 cm for n_{e2}

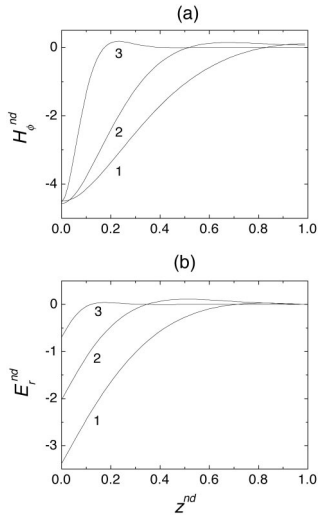

FIG. 4. Nondimensional azimuthal component of magnetic field $H_\phi^{nd} = \mathrm{Re}(H_\phi)c/\mathcal{J}$ (a) and radial component of electric field $E_r^{nd} = [\mathrm{Re}(E_r)c/\mathcal{J}]\times 10^3$ (b) *versus* dimensionless axial distance z^{nd} for $\phi = 45°$, and $r^{nd} = 0.3$. Other parameters and notations are the same as in Fig. 1.

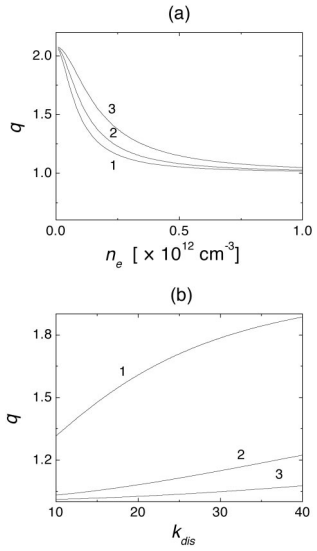

FIG. 5. Ratio q of the RF field penetration depths as a function of plasma density (a), and dimensionless collision frequency $k_{\mathrm{dis}} = \nu_{e2}/\omega$ (b). In (a), curves 1–3 correspond to $\nu_{e2}/\omega = 15$, 20, and 30, respectively. In (b), curves 1–3 are for $n_e = 10^{11}\,\mathrm{cm}^{-3}$, $5\times 10^{11}\,\mathrm{cm}^{-3}$, and $5\times 10^{12}\,\mathrm{cm}^{-3}$, respectively.

$\sim 10^{10}\,\mathrm{cm}^{-3}$, $\nu_{e2}/\omega = 30$, $R = 16$ cm, and $L = 20$ cm. In a dense plasma ($n_{e2} \sim 10^{12}\,\mathrm{cm}^{-3}$) with the other parameters remaining the same, the field is localized within the volume $z < 2.3$ cm.

We have also studied the dependence of the TE field penetration length into the chamber on the plasma parameters in the IRC and ICP discharges. Note that the field penetration is a characteristic of the RF power deposition into the chamber [1]. Figure 5 shows the ratio $q = (\gamma_1^{(2)}/\gamma_0)^{-1}$ of the field penetration lengths in the two configurations as a function of the plasma density (a) and effective collision frequency (b). Here, $\gamma_0 = [(\rho'_{01}/R)^2 - (\omega/c)^2\varepsilon_2]^{1/2}$ is the inverse field penetration length in the ICP source, where $dJ_0(\rho'_{01})/dx = 0$ [11,12]. It is clearly seen that $q \gtrsim 1$ for plasma densities $n_e < 10^{12}\,\mathrm{cm}^{-3}$. For higher plasma densities, the difference between the field penetration lengths becomes small. Thus, with respect to the field penetration the IRC configuration appears to be advantageous compared to the usual low-frequency ICP sources. Indeed, at intermediate plasma densities ($n_e \sim 10^{11}\,\mathrm{cm}^{-3}$), $(\gamma_1^{(2)})^{-1}$ can be two times larger than γ_0^{-1}. One can also expect that in the collision-dominated regime ($\nu_{ej}/\omega \gg 1$) the ratio q can effectively be controlled by the collision frequency. Fig. 5(b) shows that at intermediate densities, the penetration length in the IRC plasma is larger than that in the ICP, and their ratio increases with ν_{e2}. In fact, for $n_e \sim 10^{11}\,\mathrm{cm}^{-3}$ and $\nu_{e2}/\omega \sim 35$, the ratio q can reach 1.8.

The distribution of the magnetic field in the plasma chamber generated by the internal rotating RF current is shown in Fig. 6 for rarefied and dense plasmas. It is evident that at higher plasma densities the field is predominantly localized in the vicinity of the current plane. Furthermore, Figs. 1–5 confirm that radial uniformity of the electromagnetic fields in the IRC plasma is indeed better than in the ICP. In particular,

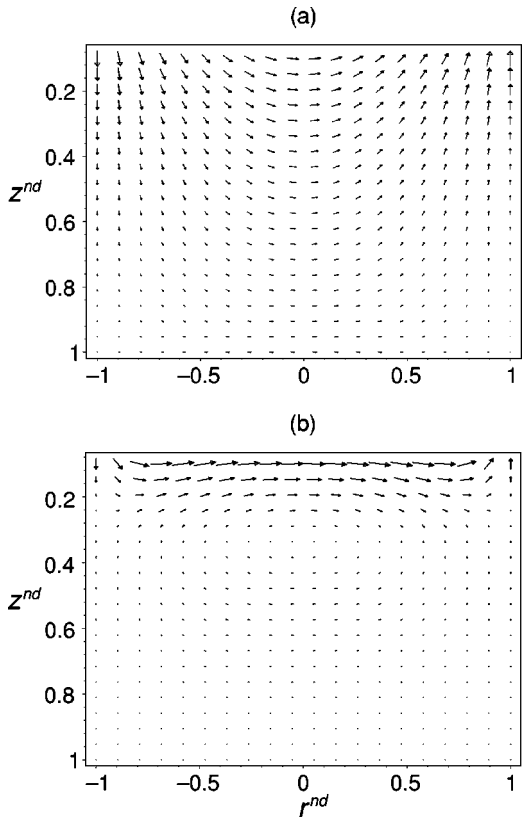

FIG. 6. Magnetic field lines in $\phi=90°$ cross section for rarefied ($n_e\sim10^9\,\mathrm{cm}^{-3}$) (a) and dense ($n_e\sim10^{12}\,\mathrm{cm}^{-3}$) (b) plasmas. The current is directed out of the paper. Other parameters are the same as in Fig. 1.

one can notice that at plasma densities $n_e\gtrsim10^{11}\,\mathrm{cm}^{-3}$, the magnetic field appears to be almost unidirectional and parallel to the interface $z=0$. Note that this is highly desirable for ion flux control in most material processing applications [1]. We recall that in the ICP sources, H_ϕ vanishes at $r=0$, which results in strong nonuniformity of power deposited near the chamber axis [11,12]. This can easily be seen in Fig. 3 of Ref. [11]. We emphasize that introduction of the rotating RF current into the plasma leads to the generation of the additional field components E_r and H_ϕ, and substantial modification of the field topography as compared to that in the ordinary ICPs.

III. POWER DEPOSITION

We now investigate the RF power transferred to plasma electrons, especially its dependence on the plasma parameters. The RF electric field induces radial and azimuthal screening currents in the plasma. In the power absorption region, which is normally of the order of the field penetration depth, the plasma electrons are heated. The neutrals can then be excited and ionized via electron-neutral collisions. Using the fluid approach, we obtain

$$P_p=\frac{1}{2}\int_0^{2\pi}\int_0^R\int_0^L \mathrm{Re}(\sigma^{(2)})|\mathbf{E}^{(2)}|^2 r\,d\phi\,dr\,dz \qquad (9)$$

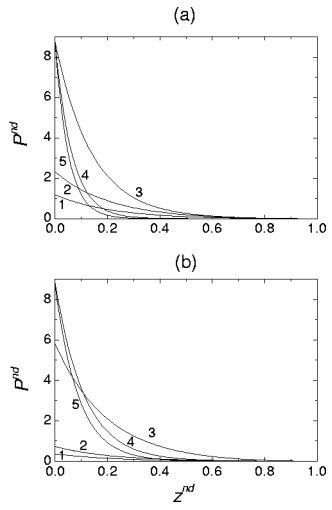

FIG. 7. Axial distribution of the dimensionless power density P^{nd} in the chamber with $R=16$ cm, $L=20$ cm, $\mathcal{L}=5$ cm, $p_0=30$ mTorr (a), $p_0=100$ mTorr (b), and $\nu_{e2}/\nu_{e1}=2$. Curves 1–5 correspond to $n_{e2}=5\times10^{10}\,\mathrm{cm}^{-3}$, $5\times10^{11}\,\mathrm{cm}^{-3}$, $5\times10^{12}\,\mathrm{cm}^{-3}$, $6\times10^{12}\,\mathrm{cm}^{-3}$, and $10^{13}\,\mathrm{cm}^{-3}$, respectively.

for the power deposited into the entire plasma volume $0<z<L$, where $\sigma^{(2)}=\omega_{p2}^2/4\pi(\nu_{e2}-i\omega)$ is the plasma conductivity, and $|\mathbf{E}^{(2)}|^2=[\mathrm{Re}(E_r^{(2)})]^2+[\mathrm{Im}(E_r^{(2)})]^2+[\mathrm{Re}(E_\phi^{(2)})]^2+[\mathrm{Im}(E_\phi^{(2)})]^2$. Equation (9) will be used in calculation of the plasma density as a function of the rotating current amplitude.

It is also useful to consider the axial dependence of the power $P_z(z)$ deposited per unit axial length averaged over the $r-\phi$ cross section. The latter can easily be obtained from (9) by removing the integral over z. Figure 7 shows the axial profiles of dimensionless power $P^{nd}=P_z(z)(c/R\mathcal{J}\sqrt{\omega})^2$ for different plasma densities and pressure.

Distribution of the RF power transferred to plasma electrons over the $r-z$ cross-section is shown in Figs. 8 and 9, for rarefied and dense plasmas, respectively. One can see that a major part of the power is deposited within the region $0<z<L/2$. If the plasma density rises, the power is mainly localized in the vicinity of the current plane. One can also deduce that the RF power can be deposited into the chamber 1.2–1.5 times deeper than in the ICPs of the same size and operating frequency [12].

We note that in dense plasmas it appears to be possible to achieve very good radial uniformity in a relatively modest region $z^{nd}<0.2$.

It should be noted that in the usual ICPs the power transferred to the plasma electrons is strongly nonuniform near the chamber axis [Figs. 8(b) and 9(b)]. Similar nonuniformity in the power contours in low-frequency ICPs have been reported earlier (Fig. 12 of Ref. [11]). Thus, the IRC configuration seems to be more advantageous for large-area plasma processing. Furthermore, the uniformity of the power density improves as the plasma density increases (Figs. 8 and 9).

Figure 10 shows the dimensionless total power absorbed by the plasma $P_p^{nd}=P_p(c/R\mathcal{J}\sqrt{\omega})^2$ as a function of the

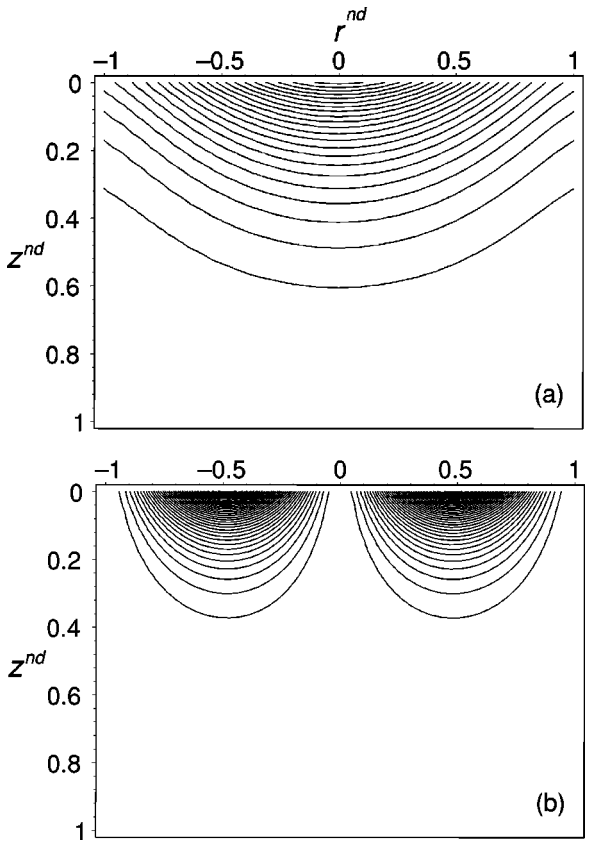

FIG. 8. Contours of the power density in the chamber filled by rarefied ($n_{e2}\sim 10^9\,\mathrm{cm}^{-3}$) plasmas for the IRC (a) and the usual ICP (b) configurations. Here, ν_{e1}, ν_{e2}, n_{e1}, and n_{e2} are the same as in Fig. 1.

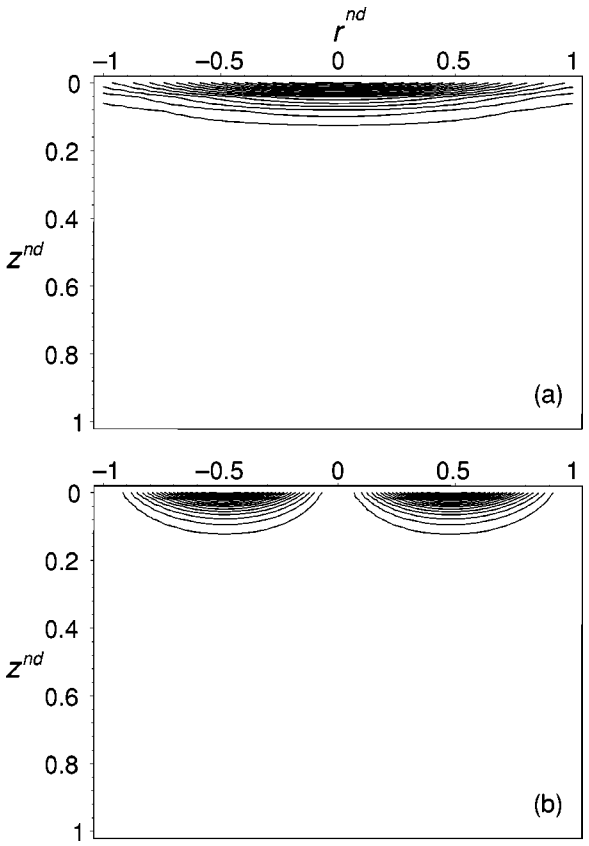

FIG. 9. Same as in Fig. 8, but for dense ($n_{e2}\sim 6\times 10^{12}\,\mathrm{cm}^{-3}$) plasmas.

plasma density and gas pressure. We note that P_p rises with the pressure, which is consistent with (9). This also indicates that P_p is an increasing function of the electron collision frequency ν_{e2}. At low plasma densities, power deposited onto the plasma rises with n_e, while at higher densities it starts to decline at $n_e\sim 5\times 10^{11}\,\mathrm{cm}^{-3}$. In particular, at $p_0=30$ mTorr the flex point corresponds to $n_e\sim 6.3\times 10^{11}\,\mathrm{cm}^{-3}$, and has a tendency to increase with pressure.

IV. POWER AND PARTICLE BALANCE

We now consider the RF power necessary to sustain an argon plasma of desired density under given discharge parameters. This can be done using the stationary power and particle balance equations

$$P_p = P_{\mathrm{loss}}, \tag{10}$$

$$\nabla(D_a \nabla n_e) - \nu_i n_e = 0, \tag{11}$$

where $P_{\mathrm{loss}}=n_v V_p \theta_p$ is the power lost by the electrons for sustaining the plasma with the spatially averaged density n_v in the volume V_p. Here,

$$\theta_p = e[\,\nu_i(\epsilon_i + 3T_e) + \nu_{4s}\epsilon_{4s} + \nu_{4p}\epsilon_{4p}]$$

is the total loss per electron–ion pair in the discharge [5]. This includes the power losses in ionization, excitation of neutral gas to the $4s$ and $4p$ states, thermal motion, and flows of plasma particles through the sheaths to the chamber walls. The ionization and excitation rates in argon are [13]

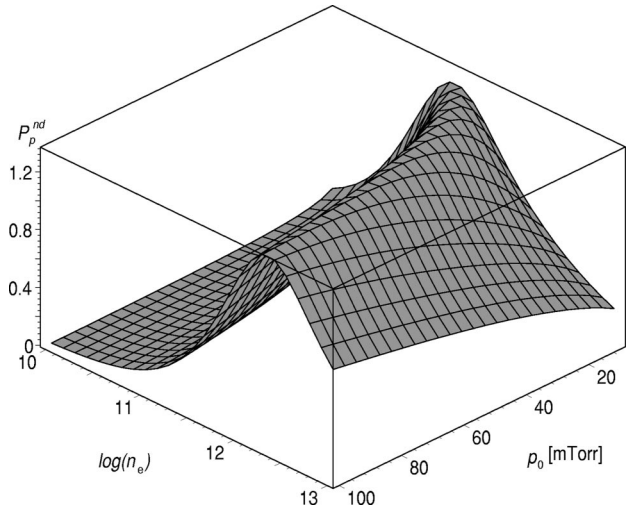

FIG. 10. 3D plot of the dimensionless power transferred to plasma electrons as a function of the plasma density and gas pressure. The chamber sizes are the same as in Fig. 7, ν_{e2}/ν_{e1} and n_{e2}/n_{e1} are the same as in Fig. 1.

$$\nu_i = 8.13\times 10^8 T_e^{0.68} p_0 \exp(-\epsilon_i/T_e),$$

$$\nu_{4s} = 1.77\times 10^8 T_e^{0.74} p_0 \exp(-\epsilon_{4s}/T_e),$$

$$\nu_{4s} = 4.95\times 10^8 T_e^{0.71} p_0 \exp(-\epsilon_{4p}/T_e),$$

where $\epsilon_i = 15.76$ eV, $\epsilon_{4s} = 11.56$ eV, and $\epsilon_{4p} = 13.2$ eV are the ionization and excitation thresholds, respectively. Here, T_e is in units of eV and p_0 is in Torr. In (11), $D_a \sim T_e \mu_i / e$ is the ambipolar diffusion coefficient, $\mu_i \sim e/m_i \nu_{in}$ is the ion mobility, m_i and ν_{in} are the ion mass and rate of ion-neutral collisions, respectively. In the above, we have assumed that the ambipolar diffusion is dominant for particle loss. This implies a limitation on gas pressure range for which our results are valid. Normally, this assumption is satisfied if the argon pressure is less than a few hundred mTorr [14].

From (11) it follows that the stationary state exists if the ionization gain is balanced by the diffusion loss, i.e., $D_a(T_e)/l_{\rm diff}^2 = \nu_i(T_e)$, where $l_{\rm diff} = (\chi^2 + \gamma_z^2)^{-1/2}$ is the effective diffusion length. We also account for the narrow plasma sheaths near the chamber walls by imposing the boundary conditions $\Gamma_r(r=R) = \Gamma_z(z=L) = \Gamma_z(z=0-) = n_s u_B$, and $\Gamma_z(z=-\mathcal{L}) = \Gamma_z(z=0+) = -n_s u_B$, where $u_B = (T_e/m_i)^{1/2}$ and n_s are ion velocity and density at the sheath edge, respectively. Here, $\Gamma_r = -D_a \partial_r n_e$ and $\Gamma_z = -D_a \partial_z n_e$ are radial and axial ion fluxes, respectively [15]. With the above boundary conditions, one can obtain from Eq. (11) the approximate plasma density profile

$$n_e(r,z) = n_{e0} J_0(\chi r) \cos[\gamma_z (z - L/2)], \tag{12}$$

where T_e, χ, and γ_z satisfy

$$\gamma_z^2 + \chi^2 = \nu_i(T_e)/D_a(T_e),$$

$$\gamma_z \tanh(\gamma_z L/2) = u_B(T_e)/D_a(T_e),$$

and

$$\chi J_1(\chi R)/J_0(\chi R) = u_B(T_e)/D_a(T_e)$$

simultaneously. The electron temperature as a function of the gas pressure and chamber geometry are obtained using the iteration. Figure. 11 shows the electron temperature versus argon pressure for different ion-neutral collision cross sections. It is seen that there is a tendency for T_e to decline with pressure, which is consistent with numerical and experimental studies of RF discharges in argon [13,15,16].

In Fig. 11, we have also included the experimental points from our earlier experiments on 500 kHz ICPs in the same chamber [12].

Note that in the figure the theoretical and experimental results correspond to rather different RF current inputs. We can thus expect similar dependence of $T_e(p_0)$ in other experiments on IRC plasmas. We note that the experimental data in Fig. 11 were also used in selecting the most suitable cross-section data and in improving the accuracy in computing the discharge operation regimes. Likewise, we find that at fixed pressure T_e is a slowly decreasing function of σ_{in}. In particular, at $p_0 = 22$ mTorr, the change of the ion-neutral

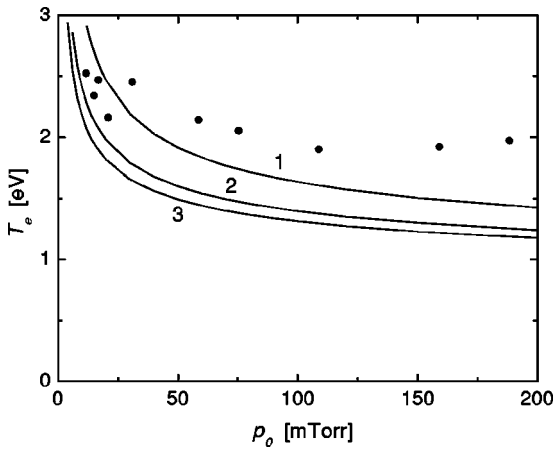

FIG. 11. Electron density versus argon gas pressure for $\sigma_{in} \sim 10^{-15}\,\mathrm{cm}^{-3}$ (1), $5\times 10^{-15}\,\mathrm{cm}^{-3}$ (2), and $5\times 10^{-14}\,\mathrm{cm}^{-3}$ (3), respectively. The other parameters are the same as in Fig. 1. Experimental points (dots) have been taken from Ref. [12].

impact cross section from $\sim 10^{-15}\,\mathrm{cm}^2$ to $\sim 10^{-14}\,\mathrm{cm}^2$ results in a reduction of the electron temperature at ~ 0.6 eV. This is consistent with the global model of argon discharge, which suggests that the electron temperature is a function of the pressure and geometry of the system [16].

The dependence of the electron temperature and effective diffusion length on the sheath width d is displayed in Fig. 12 for two different pressures. We conclude that T_e is weakly affected by the sheath width, while the effective diffusion length slowly decreases with d.

From (10), one can obtain the spatially averaged plasma density for given discharge control parameters. Alternatively, Eq. (10) yields the minimum power deposition to sustain the discharge with the desired plasma density. Figures 13 and 14 show the dependence of the power absorbed (P_p) and lost ($P_{\rm loss}$) by electrons on the plasma density in the chamber with $R = 16$ cm, $L = 20$ cm, and $\mathcal{L} = 5$ cm, for dif-

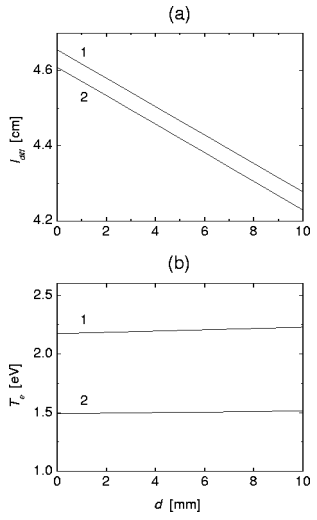

FIG. 12. Effective diffusion length (a) and electron temperature (b) versus sheath width for $\sigma_{in} \sim 10^{14}\,\mathrm{cm}^{-3}$ and gas pressures $p_0 = 10$ mTorr (curve 1), and $p_0 = 50$ mTorr (curve 2), respectively.

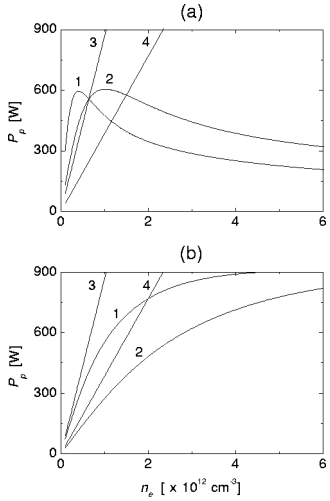

FIG. 13. P_p (curves 1 and 2) and $P_{\rm loss}$ (curves 3 and 4) for 20 mTorr (curves 1 and 3) and 50 mTorr (curves 2 and 4) argon IRC plasmas (a) and ICPs with $I_0=15$ A (b). Ratios ν_{e2}/ν_{e1} and n_{e2}/n_{e1} are the same as in Fig. 1.

ferent RF current and argon pressure. Figs. 13(b) and 14(b) correspond to the ICP configuration, with the same R, L, the azimuthal RF current at $z=-\Delta$, and a dielectric window at $-\Delta<z<0$ [12]. The width Δ and permittivity ϵ_d of the dielectric are 2.5 cm and 4.52, respectively [17]. The intersections of the curves 1 and 3 yield the minimal power and spatially averaged plasma density of the 20 mTorr discharge. Analogously, the operating regimes of the $p_0=50$ mTorr RF discharge are obtained from the intersection of curves 2 and 4.

One can see that the curves $P_p(n_e)$ and $P_{\rm loss}(n_e)$ in Fig. 13(b) do not intersect at $I_0=15$ A, which means that an ICP discharge cannot be sustained under this set of parameters. However, for the IRC case a plasma with $n_e\sim 7\times10^{11}\,{\rm cm}^{-3}$ at $I_0=15$ A and $p_0=20$ mTorr can be produced with only $\sim$550 W of RF power. At the same pressure, the rotating RF current $I_0=20$ A generates a dense ($n_e\sim10^{12}\,{\rm cm}^{-3}$) plasma with 850 W RF power. At $p_0=50$ mTorr pressure, the electron density is $n_e\sim2.3\times10^{12}\,{\rm cm}^{-3}$, and $\sim$880 W of RF power are required. We emphasise that the ICP cannot be produced with RF currents lower than $\sim$20 A, while the plasma in the IRCC can be generated with the internal RF currents as low as $\sim$9 A. Moreover, similar values of the electron number density in the ICP are achieved with higher RF powers. In particular, at $p_0=20$ mTorr, and $I_0=20$ A, $P_p\sim1.15$ kW of RF power are necessary to sustain the inductively coupled plasma.

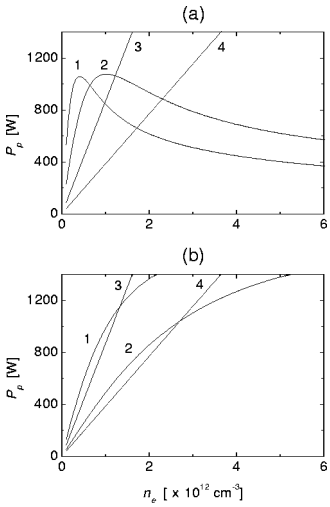

FIG. 14. Same as in Fig. 13, for $I_0=20$ A.

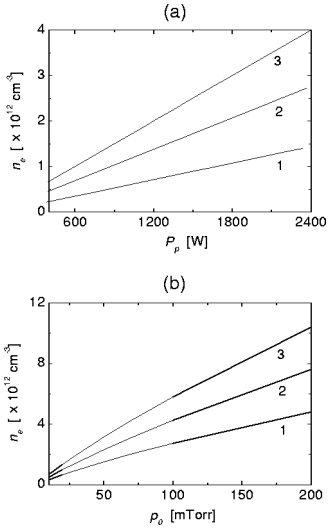

FIG. 15. Spatially averaged plasma density as a function of the input power (a) and argon pressure (b). Curves 1–3 (a) are for $p_0=10$, 20, and 30 mTorr, respectively. In (b), curves 1–3 correspond to $I_0=15$ A, 20 A, and 25 A, respectively. Ratios ν_{e2}/ν_{e1} and n_{e2}/n_{e1} are the same as in Fig. 1.

A similar procedure allows one to obtain the dependence of the spatially averaged plasma density on the input power. The results are given in Fig. 15(a). One can see that the plasma density rises monotonical with power, which is intrinsic for most low-temperature plasmas [18]. We remark that the computed values of n_e in the configuration with rotating internal current appear to be comparable with the measured plasma density in low-frequency ICP sources [12], with the same power deposited to the plasma. As can be seen from Fig. 15(b), the electron density increases with pressure, and at $p_0\sim200$ mTorr, one can achieve electron densities $\sim10^{13}\,{\rm cm}^{-3}$.

Our model suggests that RF plasmas with densities $n_e\sim10^{13}$ can be produced in the IRC configuration with reasonably low powers. This can be seen in Fig. 16, which shows the profile of the plasma density produced with 861 W of RF power. Plasma density profiles for other discharge control parameters can be computed analogously.

V. DISCUSSION

We now discuss in more detail the assumptions and limitations of our theory, and pinpoint the major effects of the internal rotating RF current on the field distribution, power deposition, and plasma parameters. For our theory, we used the conservation laws of classical electrodynamics [10], fluid

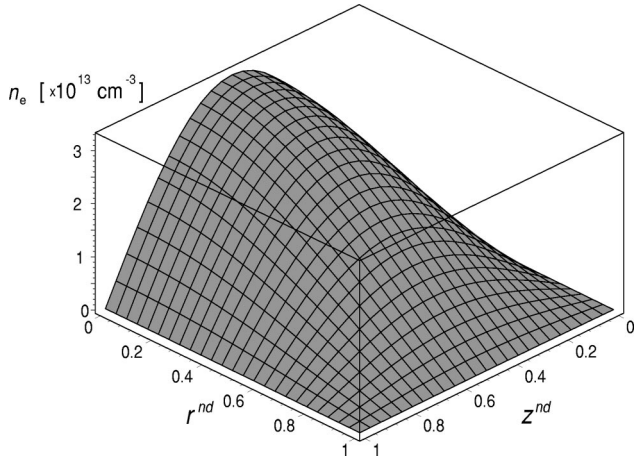

FIG. 16. Approximate plasma density profile in a chamber for $p_0=30$ mTorr, $I_0=20$ A, and $P_p=861$ W. Ratios ν_{e2}/ν_{e1} and n_{e2}/n_{e1} are the same as in Fig. 1.

plasma theory [18], and the assumptions of the global (spatially averaged) discharge model [16]. The fluid equations are used in obtaining the plasma permittivity, formulating the boundary conditions at the sheath edges, and obtaining the approximate plasma density profiles. At the same time, the global approach is used to deduce the spatially averaged (over the volume V_p) plasma density n_v from the power balance equation. Thus, the plasma densities n_v in (10) and n_0 in (12) are linked through the simple relation $n_v = V_p^{-1}\int_{V_p} n_e\, dV$, where dV is the volume element. We note that the spatially averaged model ignores the presence of metastables, and the electron temperature is a function of the pressure and geometry of the system [16].

The electromagnetic fields have been calculated assuming that the plasma is uniform. Earlier experiments on low-frequency ICPs [11,12] indicated that the plasma density is fairly uniform in the radial direction, and decreases with the axial distance. Hence, the accuracy of the present model can be improved by using self-consistent 3D nonuniform plasma density profiles, i.e., substituting (12) into (2) and (3). The field topography, power density, and the ionization rate can then be obtained accordingly.

We should mention that the current plane $z=0$ divides the chamber into two different volumes, with the sharp interface. This assumption is justified if the width of the transition layer between the two plasma volumes is smaller than the penetration length of the electromagnetic field. To make a model feasible, we did not account for a finite width (inevitable in a real experiment) of the current sheet separating regions 1 and 2, and introduced a weak density discontinuity at $z=0$. The reliable experimental data on plasma densities n_1 and n_2 are not available yet, and $n_2/n_1 \sim 1.22$ was used as a plausible guess. Indeed, since $\mathcal{L}<L$, the diffusion losses should be higher in volume 1 [1]. If one assumes that the ionization rates in volumes 1 and 2 are the same, the electron density can appear somehow lower in volume 1.

Furthermore, experimentally measured plasma densities in low-frequency ICPs appear to be consistently higher than the theoretical predictions [12]. One can expect similar results for the IRC configuration. This discrepancy can be attributed to a number of elementary processes that are neglected in the particle and power balance equations. For instance, the stepwise ionization under certain conditions can raise the argon plasma density up to 40% [13], and should therefore be accounted for in future IRC discharge models.

Another factor that can strongly affect the power deposition and particle balance is the plasma nonlinearity, often invoked for explaining the steady-state current drive in Rotamak devices [3]. In particular, we expect that strong ponderomotive forces [19] can generate axial screening currents and enhance the field penetration into the chamber. This can improve the axial uniformity of the plasma density, which has recently become a concern for processes that require a high level of plasma uniformity in large volumes [20]. Likewise, magnetic fields induced in the chamber can affect diffusion of the plasma particles, ion fluxes, and boundary conditions at the sheath edges. Hence, our results may not be valid if the RF magnetic fields generated in the chamber are too strong.

We now discuss the major advantages of the IRC configuration over the usual low-frequency ICP sources. As mentioned above, the ICP power density is strongly nonuniform near the chamber axis [11,12]. Moreover, it has recently been reported that the maxima of the optical emission intensities of the argon ions in the ICPs are away from the chamber axis, and coincide reasonably well with the maxima of the power density [21]. Thus, the ICP density appears to be nonuniform in the radial direction. Also, in the flat spiral inductive coil configuration, the actual driver currents are not purely azimuthal, as assumed in most theoretical models. Above all, the coil configuration and driving network of the ICPs are such that the plasma is inherently nonuniform and upscaling of these devices could be very inefficient [9]. In addition, ICPs possess other drawbacks, such as generation of useless RF magnetic fields outside the chamber, low power efficiency, standing-wave effects in large-area processing reactors, and relatively poor field penetration at plasma densities $n_e \gtrsim 10^{11}\,\mathrm{cm}^{-3}$ [9].

Introducing the IRC into the plasma can significantly improve the uniformity of the electromagnetic fields and RF power density in the chamber. This can be achieved by operating at a different, dipolar ($m=1$) RF resonator mode, featuring five electromagnetic field components instead of the usual three in ordinary ICPs. Moreover, the rotating unidirectional current appears to be a factor in improving the uniformity of power deposition over the cylinder cross section. We have demonstrated that at intermediate plasma densities, the electromagnetic field penetrates deeper into IRC plasmas than ICPs with the same sizes and plasma density. This should certainly improve the axial uniformity of the plasma.

The computed IRC discharge operating parameters reveal the possibility to produce higher-density plasmas with the same, or even lower, RF currents. In particular, we expect that the IRC discharge can be sustained in certain RF current range, where the ICP cannot operate. Near the current plane, plasma densities as high as $\sim 10^{13}\,\mathrm{cm}^{-3}$ can be achieved with RF powers ~ 2.5 kW.

In the paper, we have considered the electromagnetic (H) discharge regime. At low powers, the discharge normally starts with the electrostatic (E) mode. Physically, this introduces capacitive coupling and additional stochastic electron heating from interaction with the oscillating sheath, which can affect the total power balance [22]. Variation of the RF power or gas pressure can also result in mode ($E \leftrightarrow H$) transitions [23–27]. However, experiments [25,26] show that internal coil configurations are less affected by the mode jumps, and under certain conditions mode transitions can even be smooth. Note that the $E \rightarrow H$ transitions are normally abrupt in the ICPs [24]. It is thus of interest to obtain experimental results on mode transitions in IRC plasmas.

VI. SUMMARY

The effect of internal rotating currents on inductively coupled plasmas in a cylindrical metal vessel has been studied. We have derived the electromagnetic fields and power density in the chamber. Power balance has been used to obtain the spatially averaged plasma density as a function of power input. Operating parameters of the discharge and approximate plasma profiles have been computed. It is demonstrated that the uniformity of the electromagnetic fields and power density can be noticeably improved by introducing the IRC. It has also been shown that similar, or even higher than in the ICP, plasma densities can be produced under lower RF currents and the same power. Our results are thus useful for improving the uniformity of ICPs. Experiments for verifying these points are in progress and the results will be reported elsewhere.

ACKNOWLEDGMENTS

Helpful discussions with G. Collins and H. Sugai are kindly appreciated. This work was partially supported by AcRF Grants Nos. RG19/97, AcRF SX 19/97, RP 4/99 SX, SFB 191 Niedertemperatur Plasmen, Australian Research Council, and the Japan Society for the Promotion of Science. E. L. T. acknowledges the financial support of the NTU Research Scholarship. K. N. O. thanks R. Storer for hospitality at the Flinders University of South Australia.

[1] M. A. Lieberman and A. J. Lichtenberg, *Principles of Plasma Discharges and Materials Processing* (Wiley, New York, 1994).
[2] F.F. Chen, Phys. Plasmas **2**, 2164 (1995).
[3] I.R. Jones, Phys. Plasmas **6**, 1950 (1999).
[4] J. Hopwood, Plasma Sources Sci. Technol. **1**, 109 (1992); J.H. Keller, *ibid.* **5**, 166 (1996); Plasma Phys. Controlled Fusion **39**, A437 (1997).
[5] R.W. Boswell and F.F. Chen, IEEE Trans. Plasma Sci. **25**, 1229 (1997).
[6] I.R. Jones, C. Deng, I.M. El-Fayoumi, and P. Euripides, Phys. Rev. Lett. **81**, 2072 (1998).
[7] S. Xu, W. Luo, K.N. Ostrikov, J. Ahn, and S. Lee, Plasma Phys. Controlled Fusion **42**, 807 (2000).
[8] S. Xu and K.N. Ostrikov, Phys. Plasmas **7**, 3101 (2000).
[9] Y. Wu and M.A. Lieberman, Appl. Phys. Lett. **72**, 777 (1998).
[10] J. D. Jackson, *Classical Electrodynamics* (Wiley, New York, 1967).
[11] I.M. El-Fayoumi and I.R. Jones, Plasma Sources Sci. Technol. **7**, 162 (1998).
[12] S. Xu, K.N. Ostrikov, W. Luo, and S. Lee, J. Vac. Sci. Technol. A **18**, 2185 (2000).
[13] S. Ashida, C. Lee, and M.A. Lieberman, J. Vac. Sci. Technol. A **13**, 2498 (1995).
[14] K.N. Ostrikov, M.Y. Yu, and N.A. Azarenkov, J. Appl. Phys. **84**, 4176 (1998); K.N. Ostrikov, M.Y. Yu, and H. Sugai, *ibid.* **86**, 2425 (1999).
[15] V. Vahedi, M.A. Lieberman, G. DiPeso, T.D. Rognlien, and D. Hewett, J. Appl. Phys. **78**, 1446 (1995).
[16] C. Lee and M.A. Lieberman, J. Vac. Sci. Technol. A **13**, 368 (1995).
[17] In reality, $\Delta = 2.5$ cm is a combined thickness of the fused silica window (1.5 cm) and an air gap beneath the RF coil plane [12]. For simplicity, the air gap has been neglected.
[18] V. E. Golant, A. P. Zhilinsky, and I. E. Sakharov, *Fundamentals of Plasma Physics* (Wiley, New York, 1980).
[19] R.B. Piejak and V.A. Godyak, Appl. Phys. Lett. **76**, 2188 (2000).
[20] G. Collins (private communication).
[21] A.B.M. Shafiul Azam, K.N. Ostrikov, S. Xu, Y. Li, and S. Lee, Sing. J. Phys. I **16**, 56 (2000).
[22] V.A. Godyak, R.B. Piejak, B.M. Alexandrovich, and V.I. Kolobov, Phys. Plasmas **6**, 1804 (1999).
[23] U. Kortshagen, N.D. Gibson, and J.E. Lawler, J. Phys. D **29**, 1224 (1996).
[24] I.M. El-Fayoumi, I.R. Jones, and M.M. Turner, Plasma Sources Sci. Technol. **7**, 3082 (1998).
[25] K. Suzuki, K. Nakmura, H. Ohkubo, and H. Sugai, Plasma Sources Sci. Technol. **7**, 13 (1998).
[26] G. Cunge, B. Crowley, D. Vender, and M.M. Turner, Plasma Sources Sci. Technol. **8**, 576 (1999).
[27] M.M. Turner and M.A. Lieberman, Plasma Sources Sci. Technol. **8**, 313 (1999).